Crystal Structure of a Polyhistidine-Tagged Recombinant Catalytic Subunit of cAMP-Dependent Protein Kinase Complexed with the Peptide Inhibitor PKI(5−24) and Adenosine†

Narendra Narayana,‡ Sarah Cox,‡,§ Shmuel Shaltiel,|| Susan S. Taylor,*,‡ and Nguyen-huu Xuong⊥

Departments of Chemistry and Biochemistry, Biology, and Physics, University of California, San Diego, 9500 Gilman Drive, La Jolla, California 92093-0654, and Department of Biological Regulation, The Weizmann Institute of Science, Rehovot 76100, Israel

Received August 5, 1996; Revised Manuscript Received December 16, 1996⊗

ABSTRACT: The crystal structure of the hexahistidine-tagged mouse recombinant catalytic subunit (H_6-rC) of cAMP-dependent protein kinase (cAPK), complexed with a 20-residue peptide inhibitor from the heat-stable protein kinase inhibitor PKI(5−24) and adenosine, was determined at 2.2 Å resolution. Novel crystallization conditions were required to grow the ternary complex crystals. The structure was refined to a final crystallographic *R*-factor of 18.2% with good stereochemical parameters. The "active" enzyme adopts a "closed" conformation as found in rC:PKI(5−24) [Knighton et al. (1991a,b) *Science 253*, 407−414, 414−420] and packs in a similar manner with the peptide providing a major contact surface. This structure clearly defines the subsites of the unique nucleotide binding site found in the protein kinase family. The adenosine occupies a mostly hydrophobic pocket at the base of the cleft between the two lobes and is completely buried. The missing triphosphate moiety of ATP is filled with a water molecule (Wtr 415) which replaces the γ-phosphate of ATP. The glycine-rich loop between β1 and β2 helps to anchor the phosphates while the ribose ring is buried beneath β-strand 2. Another ordered water molecule (Wtr 375) is pentacoordinated with polar atoms from adenosine, Leu 49 in β-strand 1, Glu 127 in the linker strand between the two lobes, Tyr 330, and a third water molecule, Wtr 359. The conserved nucleotide fold can be defined as a lid comprised of β-strand 1, the glycine-rich loop, and β-strand 2. The adenine ring is buried beneath β-strand 1 and the linker strand (120−127) that joins the small and large lobes. The C-terminal tail containing Tyr 330, a segment that lies outside the conserved core, covers this fold and anchors it in a closed conformation. The main-chain atoms of the flexible glycine-rich loop (residues 50−55) in the ATP binding domain have a mean *B*-factor of 41.4 Å^2. This loop is quite mobile, in striking contrast to the other conserved loops that converge at the active site cleft. The catalytic loop (residues 166−171) and the Mg^{2+} positioning loop (residues 184−186) are a stable part of the large lobe and have low *B*-factors in all structures solved to date. The stability of the glycine-rich loop is highly dependent on the ligands that occupy the active site cleft with maximum stability achieved in the ternary complex containing Mg·ATP and the peptide inhibitor. In this ternary complex the γ-phosphate is secured between both lobes by hydrogen bonds to the backbone amide of Ser 53 in the glycine-rich loop and the amino group of Lys 168 in the catalytic loop. In the adenosine ternary complex the water molecule replacing the γ-phosphate hydrogen bonds between Lys 168 and Asp 166 and makes no contact with the small lobe. This glycine-rich loop is thus the most mobile component of the active site cleft, with the tip of the loop being highly sensitive to what occupies the γ-subsite.

The catalytic (C) subunit of cAMP-dependent protein kinase (cAPK), one of the smallest and simplest members of the protein kinase family (Hanks & Hunter, 1995), serves as a prototype for the large and very diverse enzyme family (Taylor et al., 1992). Its simplicity derives from its mechanism of activation whereby in the absence of cAMP it is sequestered as a fully phosphorylated protein in an inactive complex with regulatory (R) subunits. Binding of cAMP to R triggers release of the active C-subunits. The biochemical, kinetic, and structural analyses of the C-subunit have contributed significantly to our understanding of general protein kinase function.

The C-subunit of cAPK is not only the first protein kinase structure to be solved but it is still the only structure of an active protein kinase which has been cocrystallized with both peptide and nucleotide substrates. The enzyme is bilobal, with the smaller amino-terminal lobe constituting a unique nucleotide binding domain and the larger lobe providing residues important for peptide binding and catalysis. The nucleotide is buried at the base of the cleft, with the phosphates extending to the edge of the cleft where the peptide binds.

† Supported by grants from the National Institutes of Health (GM19301) to S.S.T., the National Center for Research Resources (NIH, RR01644) to N.X., the Markey Foundation to S.S.T. and N.X., and the Minerva Foundation, Munich, Germany, to S.S.

* Corresponding author.

‡ Department of Chemistry and Biochemistry, UCSD.

§ Present address: DuPont Merck Pharmaceutical Co., Experimental Station, E336/36A, Route 141 and Henry Clay Rd., Wilmington, DE 19880-0361.

|| The Weizmann Institute of Science.

⊥ Departments of Biology, Physics, and Chemistry and Biochemistry, UCSD.

⊗ Abstract published in *Advance ACS Abstracts,* April 1, 1997.

S0006-2960(96)01947-2 CCC: $14.00

The combination of structures of binary and ternary complexes of the C-subunit containing both substrate and inhibitor peptides provides a foundation for understanding the mechanism of catalysis whereby a set of highly conserved residues converge at the active site to facilitate phosphoryl transfer (Madhusudan et al., 1994). The nucleotide base is buried in a mostly hydrophobic pocket at the base of the cleft, while the phosphates are at the edge of the cleft, and it is here where most of the conserved residues converge. These active site residues, contributed by various parts of the molecule, are located primarily in three loops—a glycine-rich loop in the small lobe between β-strands 1 and 2, a catalytic loop in the large lobe between β-strands 6 and 7, and a Mg^{2+} positioning loop. The various crystal structures also define the mobility of the two domains and reveal open and closed conformations. One of the binary complexes of the mammalian enzyme containing an inhibitor peptide assumes an open conformation while all of the others are closed. These closed conformations include an ADP:PKS-(5−24) complex, an ATP:PKI(5−24) complex, a phospho-PKS(5−24) complex, and a PKI(5−24) binary complex. Opening and closing of this cleft must to some extent be an intrinsic part of the catalytic mechanism. Since the actual phosphoryl transfer step is rapid (500 s^{-1}), the slower rate-limiting step (20 s^{-1}) corresponds to opening of the cleft and ADP release (Grant & Adams, 1996).

Kinetic evidence indicates that most of the energy for nucleotide binding is associated with the adenine ring, since adenine has a K_d of 30 μM which is only 3-fold higher than the K_d or K_m of Mg·ATP. Thermostability is also enhanced nearly equivalently by Mg·ATP or adenosine (Herberg, manuscript in preparation). Most protein kinase inhibitors are competitive with ATP, and it appears that occupancy of the adenine binding site is critical for these inhibitors. To further define the nucleotide binding site of cAPK and the mobility of loops at the active site cleft, a poly(His)-tagged form of the C-subunit was cocrystallized with PKI(5−24)[1] and adenosine, leaving the phosphate subsites unoccupied. Although novel conditions were required to obtain crystals, the structure assumed a closed conformation similar to earlier ones with a water molecule occupying the γ-phosphate in the active site cleft. The structured water molecules at the active site are described. Analysis of the various closed conformations reveals that the glycine-rich loop is the single mobile component of the active site cleft and assumes a fully closed and stable conformation only when Mg·ATP and the inhibitor peptide are present.

This structure of the H_6-rC shows that the fundamental features of the kinase structure are not disturbed by the His_6 tag. In the rC-subunit which lacks the N-terminal myristic acid, the first 10−15 residues are disordered. The stretch of 20 residues containing the His_6 tag is also disordered although this does not interfere with crystal packing. Nevertheless, the presence of the His_6 tag required different crystallization conditions. This is extremely important for subsequent analysis of mutants of the C-subunit that cannot be purified by conventional methods.

EXPERIMENTAL PROCEDURES

Protein, Peptide Inhibitor, and Nucleoside. The construction of the His_6-tagged mouse rC will be described elsewhere (Cox et al., manuscript in preparation). To summarize, a 20-residue peptide including six contiguous histidines was fused to the N-terminus of rC. The His_6-rC was expressed in *Escherichia coli* (Slice & Taylor, 1989) and purified using nickel chelate affinity chromatography. Isoforms were separated by chromatography on a Mono-S column as described by Herberg et al. (1993), except that dialysis was carried out in a two-step procedure, first against 20 mM potassium phosphate (pH 6.2) and 50 mM KCl and then against 20 mM potassium phosphate, pH 6.2, and 25 mM KCl, before being loaded onto the Mono-S 10/10 column (Pharmacia). The H_6-rC was resolved into three isoforms by eluting with a 25 mM−1 M KCl linear gradient. Isoform II, phosphorylated at three sites—Ser 10, Thr 197, and Ser 338 (Herberg et al., 1993)—was used for crystallization. The peptide inhibitor PKI(5−24), a 20-residue segment of the heat-stable protein kinase inhibitor (PKI) with an apparent K_i of 2.3 nM (Cheng et al., 1986), was synthesized on a Milligen peptide synthesizer and purified to homogeneity by high-performance liquid chromatography (HPLC). Adenosine was purchased from Sigma Chemical Co.

Crystallization. Since the conditions used previously for crystallizing the rC-subunit with poly(ethylene glycol) 400 (PEG-400) (Zheng et al., 1992) were unsuccessful for the H_6-rC complex, novel crystallization conditions were developed. Orthorhombic crystals of the ternary complex, comprised of mouse H_6-rC, PKI(5−24), and adenosine, were grown by the hanging-drop vapor diffusion method using 2-methyl-2,4-pentanediol (MPD) as the precipitating agent. The mother liquor (20 μL) contained protein at a concentration of 0.25 mM in 100 mM Bicine buffer at pH 8.0, 0.75 mM PKI(5−24), 4 mM adenosine, and 4% MPD. The reservoir solution (1 mL) was made up of 20% MPD in 100 mM Bicine buffer (pH 8.0). X-ray diffraction quality crystals ($0.2 \times 0.15 \times 0.8$ mm^3) were grown at 4 °C in approximately 4−6 weeks. The crystallization mixture did not contain divalent metal ions. Several trials using poly(ethylene glycol) 400 (PEG-400) as precipitant according to the protocol described in the crystallization of rC:PKI(5−24) and rC:PKI(5−24):Mg_2·ATP (Zheng et al., 1992) complexes were unsuccessful.

Data Collection. The crystals belong to the space group $P2_12_12_1$ with unit cell dimensions of $a = 73.08$ Å, $b = 78.44$ Å, and $c = 80.49$ Å. There is one ternary complex molecule per asymmetric unit (Matthews coefficient, $V_m = 2.7$ Å^3/Da; 54% crystal solvent content). X-ray intensity data on a single crystal were collected at 4 °C on Xuong−Hamlin multiwire area detectors (Hamlin, 1985), with a graphite monochromated Cu Kα beam from a Rigaku RU-200 rotating anode X-ray generator operating at 5 kW power. Data reduction was done with the UCSD area-detector data processing programs (Howard et al., 1985). The crystal diffracted to 2.2 Å resolution with an R_{sym} ($\sum|I_{obs} - I_{av}|/\sum I_{av}$) of 0.064 and 92% completeness. There was a decay of 8.0% over an X-ray exposure period of 2 days. The Wilson *B*-factor is 34 Å^2.

[1] Abbreviations: PKI(5−24) corresponds to residues 5−24 in the naturally occurring heat-stable protein kinase inhibitor (TTYADFIASGRTGRRNAIHD). PKS(5−24) represents the corresponding substrate peptide, TTYADFIASGRTGRR**AS**IHD, where the residues shown in bold were changed to NA, respectively, in the peptide inhibitor. PKS(5−24)* represents the same peptide phosphorylated at Ser 21. The complexes rC:PKI(5−24):Mn_2·ATP, rC:PKI(5−24):adenosine, rC:PKI(5−24), and mC:PKI(5−24):ATP are abbreviated as rCI·ATP, rCIA, rCI, and mCI·ATP, respectively.

Table 1: Unit Cell Dimensions of Mouse rC Complexes with the Space Group $P2_12_12_1$[a]

compound	unit cell lengths (Å)			reference
	a	*b*	*c*	
rC + PKI(5−24)	73.84	75.76	81.01	Knighton et al. (1993)
rC + PKI(5−24) + Mn_2·ATP	73.58	76.28	80.58	Zheng et al. (1993b)
rC + PKS(5−24) + ADP	73.96	76.11	81.00	Madhusudan et al. (1994)
rC + PKS(5−24)*	73.87	75.58	80.70	Madhusudan et al. (1994)
rC + PKI(5−24) + adenosine	**73.08**	**78.44**	**80.49**	this work

[a] PKI(5−24) corresponds to residues 5−24 in the naturally occurring heat-stable protein kinase inhibitor (TTYADFIASGRTGRRNAIHD). PKS(5−24) represents the corresponding substrate peptide, TTYADFIASGRTGRR**AS**IHD, where the residues shown in bold were changed to NA, respectively, in the peptide inhibitor. PKS(5−24)* represents the same peptide phosphorylated at Ser 21. The average estimated standard deviation (esd) of unit cell lengths is 0.05 Å. The esds for unit cell lengths were obtained by taking the average of the refined cell parameters for each orientation (total of seven runs) and then calculating the standard deviation for each cell axis. The mean *B*-factors for the main-chain atoms in the above listed complexes are 28, 33, 24, 29, and 38 Å^2, respectively.

Structure Refinement. The cell dimensions of the orthorhombic crystal form of different complexes of mouse rC, whose structures are reported previously, are compared in Table 1. The length of the *b*-axis in the present structure is approximately 3% longer than the corresponding axis in the other crystals. The variations in the other two dimensions (*a*- and *c*-axes) are less than 0.5% for all crystals obtained so far. This elongation along the *b*-axis is significant and was observed previously in crystals of a rC binary complex with PKI(5−24) where variations range between 75.36 and 77.61 Å, with one crystal whose *b*-axis was even more elongated (80.1 Å) (Knighton et al., personal communication). Possible reasons for the observed variation in the cell dimension along the *b*-axis are discussed further in the section pertaining to crystal packing. This is the first reported structure analysis of an rC complex grown using a precipitant other than PEG-400, and all crystals tested for X-ray diffraction during this work consistently had an elongated *b*-axis, unlike the other rC binary and ternary complexes (see Table 1).

The coordinates of the mouse rC complexed with PKI(5−24) (PDB entry 1APM) were used as the starting model for refinement against the X-ray data obtained from the present crystal of the ternary complex. The isotropic *B*-factors were set uniformly to 15 Å^2 for all protein and peptide inhibitor atoms. The model was initially subjected to rigid body refinement and was then followed by several cycles of conjugate-gradient positional and overall isotropic and individual restrained *B*-factor (thermal factor) refinement using the X-PLOR program (Brunger, 1992). The data used in these refinement cycles were gradually increased from 3.0 to 2.2 Å in three steps. Refinement of this binary model converged at a crystallographic *R*-factor of 21.6% for data ($F > 2\sigma_F$) between 10 and 2.2 Å. A difference Fourier map calculated at this stage using 20−2.2 Å data clearly showed electron density for adenosine (see Figure 1). Further refinement was continued with the inclusion of adenosine. The simulated annealing slow-cool refinement protocol was run from $T = 3000$ K down to $T = 277$ K in steps of 25 K (time step = 0.5 fs and tolerance = 0.2 Å). This refinement was followed by 40 cycles of Powell minimization, 20 cycles of overall *B*-factor refinement, and 25 cycles of restrained individual *B*-factor refinement, which converged at $R = 21.0\%$ for 10−2.2 Å resolution. A simulated annealed omit map was computed by excluding residues within a 4 Å radius of the adenosine. All omitted atoms were readily fitted into the electron density map with the aid of the molecular graphics program package TOM-FRODO (Cambillau & Horjales, 1987). Electron densities for some side-chain atoms, particularly Lys and Arg residues on the surface such as Lys 63, Lys 78, and Arg 256, that were not found in the starting model were located reliably in the present structure via several difference Fourier maps. The two C-terminal residues, His 23 and Asp 24, of the peptide inhibitor are well defined, and there was no indication of alternate conformations for any of the residues, unlike those in the binary complex structure of rC:PKI(5−24) (Knighton et al., 1993). At the completion of X-PLOR refinement, the model consisted of all atoms of the rC from residue 13 to residue 350, the peptide inhibitor PKI(5−24), and adenosine. The His_6 tag as well as residues 1−12 of the rC was not seen in the electron density maps and is assumed to be thermally disordered. All atoms have full occupancy, and their individual *B*'s refined with restraints. The target standard deviations between *B*-factors of bonded backbone and side-chain atoms were 1.5 and 2.0, respectively. The target standard deviations between *B*-factors of backbone and side-chain atoms connected by an angle were 2.0 and 2.5, respectively.

This refined model was further subjected to least-squares refinement using the conjugate-direction algorithm in the TNT program (Tronrud et al., 1987). After the convergence of the model to an *R*-factor of 20%, water molecules were built into the structure in five rounds of alternate structure refinement and identification of solvent peaks in the difference Fourier maps. Waters were assigned to peaks greater than 3σ in the difference Fourier maps and concomitantly at a hydrogen bonding distance with other polar atoms. The inclusion of 90 water molecules with an additional five cycles of refinement resulted in a final *R*-value of 18.2% for data between 10 and 2.2 Å. In the glycine-rich loop (residues 50−55), the mean *B*'s for main-chain and side-chain atoms are 41.4 and 67.3 Å^2, respectively. The unrestrained average *B* excluding atoms corresponding mostly to the surface side chains which hit the maximum allowed value of 100 Å^2 was 32.4 Å^2. The structure has good stereochemical parameters as estimated by the program PROCHECK (Laskowski et al., 1993), and there are no non-glycine residues within disallowed (ϕ, ψ) regions in a Ramachandran plot (Ramachandran & Sasisekharan, 1968). Some results pertaining to TNT refinement are summarized in Table 2.

RESULTS

The overall structure of this rCIA ternary complex assumes a closed conformation with the adenosine deeply buried in a solvent-inaccessible pocket at the base of the cleft between the two lobes. The additional 20 amino acids at the

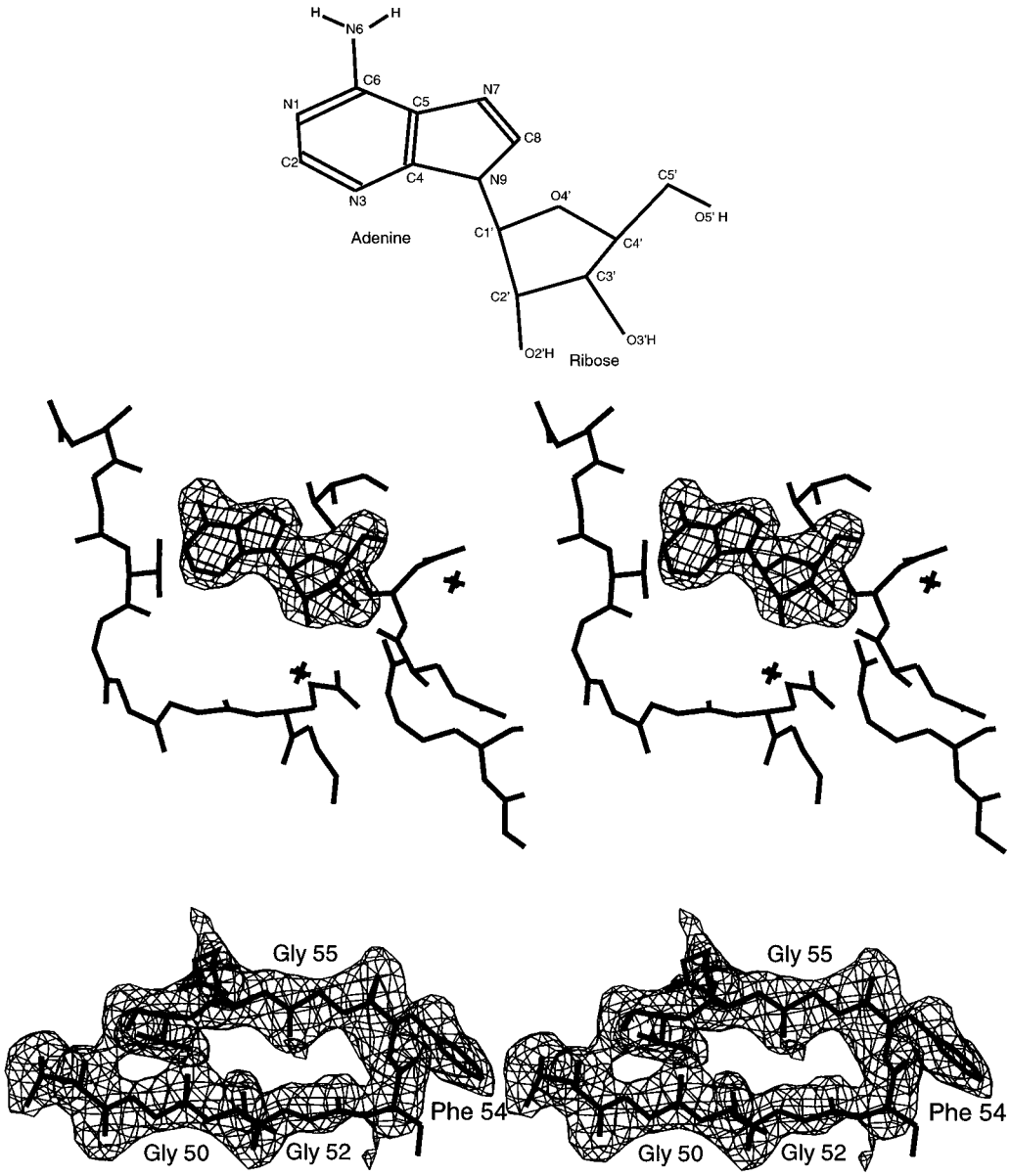

FIGURE 1: Panel a (top): Covalent structure of adenosine and atom numbering scheme. Panel b (middle): Stereoview of the electron density difference Fourier map. The map was computed using the Fourier terms $(F_o - F_c)\, e^{i\alpha}$, where F_o and F_c are observed and calculated structure factor amplitudes, respectively, and α is the calculated phase using the final TNT refined model without adenosine. The map is contoured at four standard deviations (4σ). Panel c (bottom): Stereoview of an omit map of the glycine-rich loop with the omitted residues in the map calculation superimposed on the electron density. The map is contoured at 3σ. This figure and Figures 3, 4, and 7 were made using the molecular graphics program InsightII (*InsightII User Guide*, 1994).

N-terminus including the His_6 tag as well as residues 1−12 of the C-subunit are presumably disordered and are not seen in the electron density maps. By comparing this structure with previous structures of the rC and mC complexes, we can better define the various subsites that constitute the nucleotide binding site, a motif that is unique to the protein kinase family. In addition, we have defined the ordered water molecules that are an integral part of the nucleotide binding pocket. Understanding the detailed features of this nucleotide binding domain is critical not only for understanding how the active site is configured but also for understanding how kinases, in general, are regulated. Finally, it is important for the rational design of inhibitors which mostly target this nucleotide binding pocket.

Overall Architecture. This is the first structure of an rC that contains a poly(His) tag at its N-terminus. It was extremely important to establish that this tag, which allows for rapid purification of wild type and mutant proteins, did not perturb the overall structure of the protein. This structure begins with residue 13 as does the rC structures that were solved previously. In this structure of poly(His) rC, the additional 20 residues at the N-terminus containing the His_6 tag are also disordered. There is enough room to accommodate these extra residues in this region of the crystal packing. Although the *b*-axis dimension in this structure differs by 3% compared to the rC:PKI(5−24) binary complex, nevertheless, least-squares superposition of the C^α atoms corresponding to residues 13−350 of both complexes resulted in a low rms deviation of 0.33 Å, indicating the similarity between the two complexes. The poly(His) tag, therefore, does not interfere with the overall conformation of the rC.

The enzyme adopts a "closed" conformation with a radius of gyration of 20.0 Å, as seen in the crystal structures of

Table 2: Refinement Results

model	atoms in residues e:13−e:350, i:5−i:24, adenosine, and 90 water molecules (3058 non-H atoms)
data	19980 reflections; ($F > 1\sigma_F$) in 10−2.2 Å resolution range
R-factor[a]	18.2%
mean *B*-factors (Å^2)	
main-chain atoms	38.2
side-chain atoms	46.1
water molecules	55.4
rmsds for geometrical parameters[b]	
bond lengths	0.012 Å
bond angles	2.5°
general planes	0.01 Å
trigonal planes	0.01 Å

[a] *R*-factor is defined as $100\sum|F_o - F_c|/\sum F_o$. [b] Average error in coordinates as estimated from the Luzzati plot (Luzzati, 1952) is 0.30 Å.

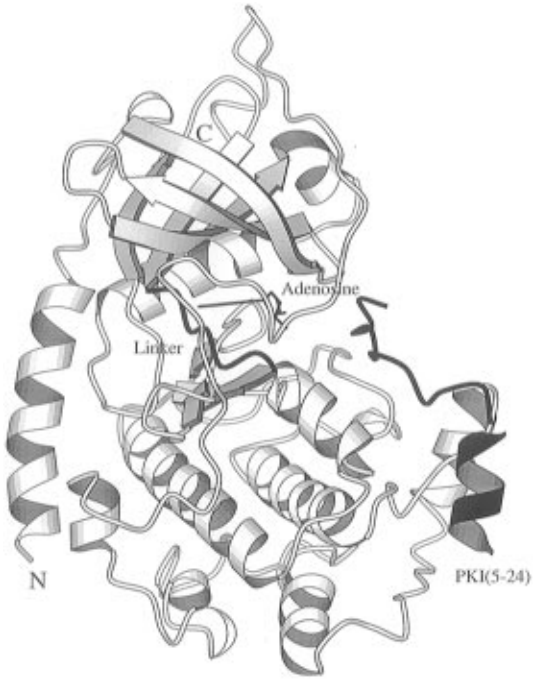

FIGURE 2: Ribbon representation of the ternary rC:PKI(5−24):adenosine structure. The adenosine, linker region (residues 120−127) between the upper N-terminal lobe and the lower C-terminal lobe of the kinase, and the peptide inhibitor PKI(5−24) are highlighted in black. The letters N and C denote N- and C-termini, respectively. This figure and Figure 5 were prepared using the program MOLSCRIPT (Kraulis, 1991).

rC:PKI(5−24) and rC:PKI(5−24):Mg_2·ATP. The secondary structure elements in the bilobal enzyme (Figure 2) are labeled according to Knighton et al. (1991a). The adenosine is buried between the large and small lobes. Access to the active site cleft is blocked by the peptide inhibitor, by the glycine-rich loop between β-strands 1 and 2, and by the enzyme's C-terminal tail segment (residues 315−335), resulting in a solvent-inaccessible enclosure for the nucleoside. The bound peptide inhibitor, PKI(5−24), contains an amphipathic helix followed by a turn and an extended region, similar to that observed in the rC:PKI(5−24) and rC:PKI(5−24):Mg_2·ATP complexes.

Geometry of the Adenosine and Its Interactions with the Protein and PKI(5−24). (A) Adenine Binding Site. Adenosine is bound to the unique protein kinase nucleotide binding fold with interactions that are essentially the same as observed in the ternary complex of rC:PKI(5−24):Mn_2·ATP (Zheng et al., 1993b) and the porcine C-subunit complexed with PKI(5−24) and Mn_2·AMP-PNP (Bossemeyer et al., 1993). The adenine base is completely buried in a hydrophobic pocket formed at the junction of the small and large lobes. The planar adenine ring is involved in numerous interactions, both hydrophobic and hydrogen bonding, with the enzyme. With only a few exceptions, these interactions involve residues that are located either in the small lobe or in the linker strand residues 120−127 that join the two lobes (Table 3). The residues involved in hydrophobic interactions are Leu 49, Val 57, Ala 70, Val 104, Met 120, Glu 121, Tyr 122, Val 123, Leu 173, Thr 183, and Phe 327. In general, the hydrophobicity of these residues is conserved throughout the protein kinase family. In addition to these interactions, the purine base forms three hydrogen bonds (see Figure 3 and Table 4). The N1 interacts with the main-chain amide of Val 123, the N6 amino group donates a hydrogen bond (H-bond) to the backbone carbonyl of Glu 121, and N7 is bonded to OG1 of Thr 183. The involvement of the N6 amino group in the hydrogen bond formation is consistent with prior analogue studies, since removal of a hydrogen bond donor at this position results in a decrease in binding affinity (Hoppe et al., 1978; Taylor et al., 1990). Replacing one of the N6 hydrogens with a methyl group has an even greater effect on K_m, which confirms the fact that the adenine ring is tightly packed in this pocket. Therefore, the tetrapeptide segment Met 120−Val 123 plays a crucial role in the recognition of the adenine base both by hydrogen-bonding and hydrophobic interactions. This segment, indicated in Figure 2, is part of the short strand (residues 120−127) that links the two domains in the conserved catalytic core. With the exception of Leu 173, Thr 183, and Phe 327, all of the residues that comprise the adenine binding pocket and are in close contact with the purine base are located in either the small lobe or the linker strand (120−127).

Table 3: Residues That Comprise the Adenosine Binding Site

residue	location	type of interaction
	Adenine Binding Site	
Leu 49	β-strand 1; small lobe	hydrophobic
Val 57	β-strand 2; small lobe	hydrophobic
Ala 70	β-strand 3; small lobe	hydrophobic
Val 104	loop between C-helix and β-4; small lobe	hydrophobic
Met 120	extended strand; linker region	hydrophobic/H-bond
Glu 121	extended strand; linker region	hydrophobic/H-bond
Tyr 122	extended strand; linker region	hydrophobic
Val 123	extended strand; linker region	hydrophobic/H-bond
Leu 173	β-strand 7; large lobe	hydrophobic
Thr 183	β-strand 8; large lobe	hydrophobic/H-bond
Phe 327	C-terminal tail	hydrophobic
	Ribose Binding Site	
Leu 49	β-strand 1; small lobe	hydrophobic
Gly 50	β-strand 1; small lobe	hydrophobic
Thr 51	β-strand 1; small lobe	hydrophobic
Val 57	β-strand 2; small lobe	hydrophobic
Glu 127	extended strand; linker region	hydrophobic/H-bond
Glu 170	catalytic loop; large lobe	hydrophobic/H-bond
Asn 171	catalytic loop; large lobe	H-bond
Asp 184	DFG loop; large lobe	hydrophobic
Arg P-3	peptide inhibitor, PKI(5−24); large lobe	hydrophobic/H-bond

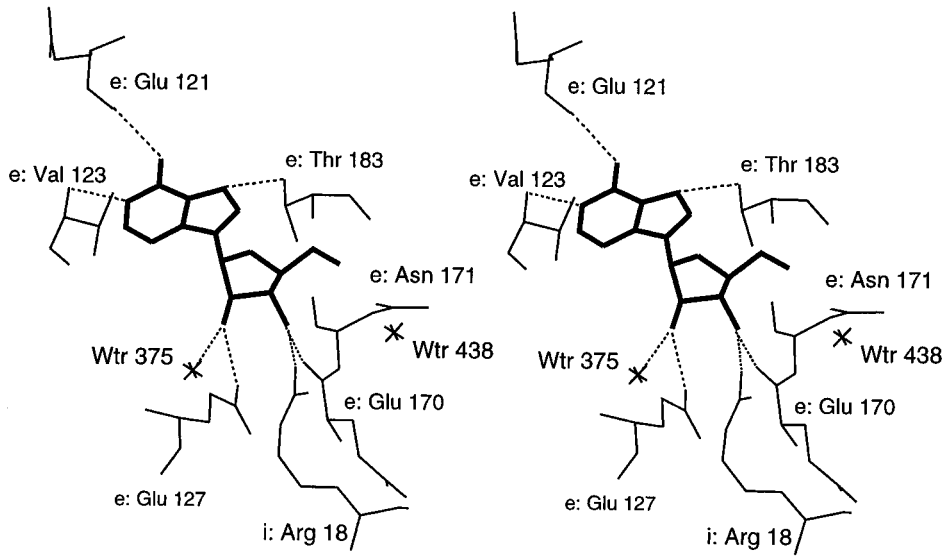

FIGURE 3: Stereoview of the adenosine binding pocket. Dashed lines represent hydrogen bonds. Adenosine and the surrounding residues are represented by thick and thin lines, respectively. The waters are denoted by the symbol *. All non-carbon interactions between adenosine and the enzyme (≤3.3 Å) are listed in Table 4.

Table 4: Non-carbon Interactions (≤3.3 Å) Involving Adenosine[a]

adenosine	rC or PKI(5−24) or waters	distance (Å)
N1	Val 123−N(e)	3.0
N6	Glu 121−O(e)	2.8
N7	Thr 183−OG1(e)	2.8
O2′	Glu 127−OE2(e)	2.4
	Arg 18−NH2(i)	3.3
	Wtr 375−O	2.8
O3′	Glu 127−OE2(e)	3.1
	Glu 170−O(e)	2.5
	Arg 18−NH2(i)	2.8
O5′	Asn 171−OD1(e)	3.3
	Wtr 438−O	3.3

[a] The letters e and i within parentheses denote the chain names of the enzyme and the peptide inhibitor, respectively. In the set of final refined coordinates, the phosphorylated residues are labeled Thp 197 and Sep 338. No density was seen for the phosphorylated Sep 10. Residues in the two polypeptide chains, rC and the peptide inhibitor, are identified by the chain names e and i, respectively. The 20-residue peptide inhibitor is labeled i:5 through i:24. Adenosine is labeled ads 351, and water molecules are numbered from 352 to 441. For ease of discussion with other related structures, the Ser 21 phosphorylation site in the substrate peptide is labeled P and sites N-terminal and C-terminal to this P-1 and P+1, etc. The complexes rC:PKI(5−24):Mn_2·ATP, rC:PKI(5−24):adenosine, rC:PKI(5−24), and mC:PKI(5−24):ATP are abbreviated rCI·ATP, rCIA, rCI, and mCI·ATP, respectively.

(B) Ribose Binding Site. The ribose adopts an unsymmetrical twist (major C3′-endo pucker) about the plane formed by atoms O4′, C1′, and C4′. The sugar assumes an *anti* conformation ($\chi = -151.7°$; Saenger, 1984) with respect to the adenine base. Unlike the purine ring, the sugar interacts with both the enzyme and the peptide inhibitor PKI(5−24). The exocyclic oxygens O2′, O3′, and O5′ are all involved in hydrogen bonding (see Figure 3 and also Table 4). As seen in the ternary complex of rC:PKI(5−24):Mn_2·ATP (Zheng et al., 1993b), the O2′ interacts with the side chain of Glu 127 while the O3′ interacts with the P-3 arginine of PKI(5−24) and the backbone carbonyl of Glu 170. In addition to these interactions, in both structures the O2′ forms a hydrogen bond with a water molecule (Wtr 375) and the O3′ is hydrogen-bonded to OE2 of Glu 127. However, the torsion angle C3′−C4′−C5′−O5′ = −38.3° is significantly different from that found in the ternary complexes rC:PKI(5−24):Mn_2·ATP (73.7°) and mC:PKI(5−24):Mn_2·AMP-PNP (61.9°). Therefore, the O5′ atom has moved significantly away from the base and the sugar ring compared to both the ternary complexes containing the phosphate groups. This O5′ atom has a *B*-factor of 76 Å^2. Rotation about the exocyclic C4′−C5′ bond allows O5′ to assume different positions relative to the base and the furanose. In purine nucleosides, the orientation about this bond is preferentially +*synclinal* (∼60°), but both −*synclinal* and *anti* (∼180°) are sometimes found (Saenger, 1984).

(C) Phosphate Binding Site. In contrast to the hydrophobic adenosine binding pocket, the binding site filled by the phosphates of ATP in the ternary rCI·ATP is very polar. In this structure all three phosphates are missing. This site is filled by a water molecule, Wtr 415, that occupies the position of the γ-phosphate of ATP. Many of the conserved residues such as Lys 72, Glu 91, and Asp 184 that cluster around this site of phosphoryl transfer do not move significantly in this structure. The crucial placement of this water molecule also means that the conserved residues do not need to move. See section on Solvent Structure in the Active Site Cleft for details.

Conformation of the Peptide Inhibitor PKI(5−24) and Its Interactions with the Protein. In this structure the peptide inhibitor PKI(5−24) is bound in a similar conformation to that described for the other rC ternary and binary complexes. The key ionic interactions between the arginines at P-2, P-3, and P-6 with glutamates 230 and 170 (P-2), 127 (P-3), and 203 (P-6) are all conserved. In addition to the interaction of the P-3 Arg with Glu 127, there is also a weak interaction with the side-chain hydroxyl of Tyr 330 (3.4 Å). This interaction was seen in the previous "closed" structures but was not emphasized. In addition, the same hydroxyl of Tyr 330 interacts with the carbonyl of Leu 49 and the 2′-OH of the ribose of adenosine, via a water bridge. Mutational studies indicate that Tyr 330 is important for both peptide binding and catalysis (Chestukhin et al., 1996). The P-3 Arg donates a hydrogen bond to the carbonyl oxygen of Thr 51 in the glycine-rich loop between β-strands 1 and 2. Also conserved in this structure are the hydrophobic interactions of the P-11 Phe with Arg 133, Gly 234, Tyr 235, Pro 236,

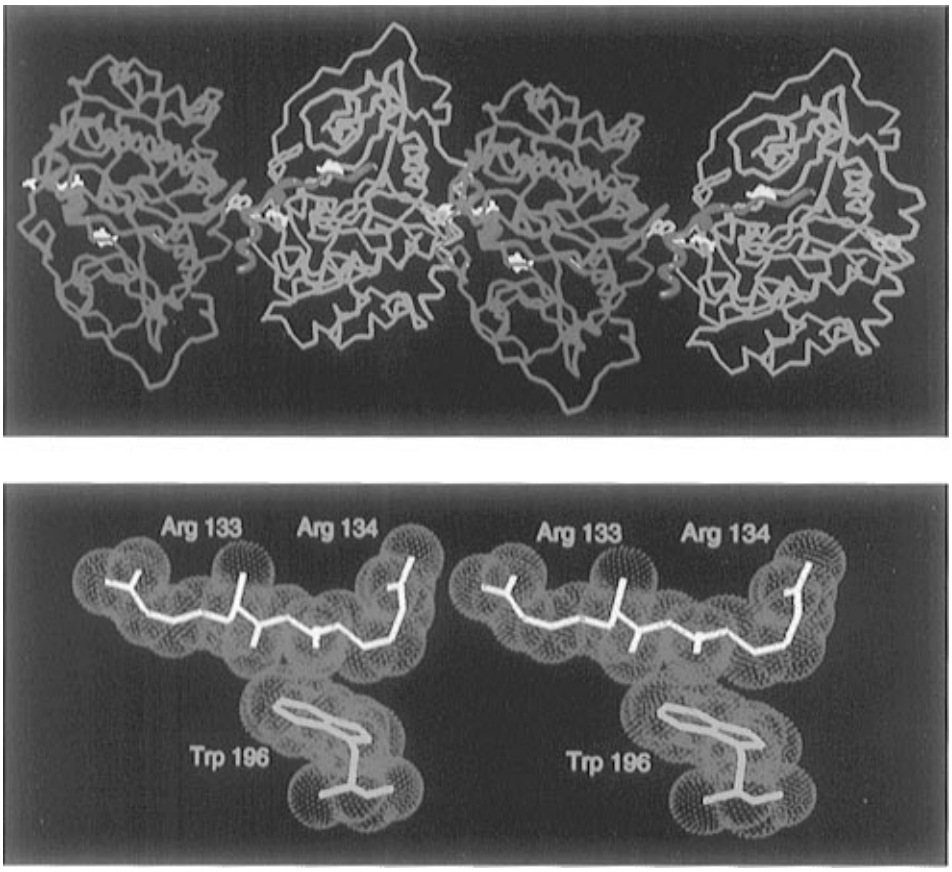

FIGURE 4: Crystal packing of the rCIA ternary complex. (a, top) Monoview of a section of the chain of the rC complex packed along the unit cell *c*-axis. The intermolecular contacts are strongly mediated by the peptide inhibitor (red). The C^{α} trace of the molecule is in magenta. Its 2_1-screw-related molecule is shown in cyan. Adenosine, Arg 133, and Arg 134 are shown in white and Trp 196 is in yellow. (b, bottom) Stereoview of the van der Waals surface of the hydrophobic interactions between the Trp 196 residue (yellow) on one molecule and Arg 133 and Arg 134 (white) of the neighboring molecule.

and Phe 239. There is a weak interaction between the C-terminal Asp of the peptide inhibitor and the side chain of Lys 83. The imidazole of the P+2 His is positioned within van der Waals distance from the side chain of Phe 54 in the glycine-rich loop. The P-site Ala is marginally closer to the enzyme active site. The distances between the hydroxyl of Ser 53 in the glycine-rich loop and P-site's backbone amide and the carbonyl oxygen are 3.2 and 2.9 Å, compared to 3.5 and 2.8 Å, respectively, in the Mn_2·ATP-containing ternary complex structure and 3.7 and 3.6 Å, respectively, in the binary complex rC:PKI(5−24). The average *B*-factors (Å^2) for Ser 53 in the rCI·ATP, mCI·ATP, rCIA, and rCI structures are 23.95, 20.40, 64.42, and 72.31, respectively.

Crystal Packing. The enzyme complex is packed in an infinite chain of molecules related by a crystallographic 2_1-axis on each of the unit cell axes directions. Intermolecular interactions may be classified into three groups based on the direction of the operating symmetry axis. The number of unique intermolecular contacts (≤4.0 Å) and hydrogen bonds generated by 2_1-axes along the unit cell *a*, *b*, and *c* directions are 25, 2; 8, 2; and 58, 7; respectively, which implies strong interactions along the *c*-direction, moderate along the *a*-direction, and weak along the *b*-direction. Residues from the peptide inhibitor are involved in all of the seven strong intermolecular hydrogen bonds and also participate in numerous hydrophobic interactions along the *c*-direction (Figure 4a). Also seen in this chain of molecules are the hydrophobic interactions between the dipeptide segment Arg 133 and Arg 134 and the symmetry-related Trp 196 (see Figure 4b). This is probably the most important direct protein−protein interaction. The electron density for these interacting residues is well defined. The hydroxyl OG1 of i:Thr 5 is involved in the formation of a "three-center" hydrogen bond with the symmetry-related carboxylate of OE1 and OE2 of Glu 86. The atom OD1 of i:Asp 9 is involved in bifurcated hydrogen bonding with NH1 and NH2 of Arg 93, also seen previously in binary and ternary structures, which crystallized in the same crystal form (Knighton et al., 1993; Zheng et al., 1993a,b). The crystal contacts along the *a*-direction also involve residues from the peptide inhibitor. The large thermal mobility of the N-terminal residues results in weak and diffused electron density. Consequently, the intermolecular hydrogen bonding interactions involving these residues along the *b*-direction are not reliable. Therefore, as indicated above, there are only a few, weak and nonspecific contacts along the *b*-direction.

The change in cell dimension along the *b*-axis by 3%, compared to other reported rC complexes in the same orthorhombic crystal form (see Table 1), may be due to the weak and few interactions along the *b*-axis and/or may have been affected by the polyhistidine tag at the amino terminus of the enzyme which is in the contact region along the *b*-axis. Another possibility for the observed change in *b*-axis could be the different crystal-growing conditions used in this analysis. The expansion in *b*-axis length did not result in significant dislocation of the molecule.

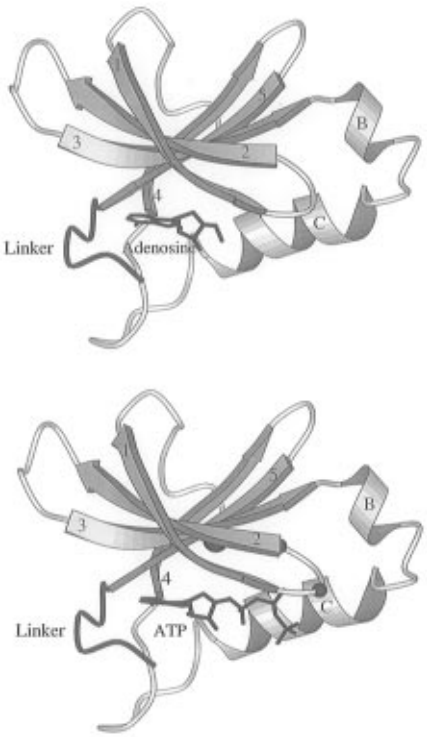

FIGURE 5: Nucleotide binding lobe. Panel a (top) shows the binding of adenosine in the hydrophobic pocket beneath the twisted β-sheet. The adenine base makes important H-bonding interactions with the linker region. Panel b (bottom) shows the binding of triphosphates below the glycine-rich loop in a very polar environment. The spheres represent the enzyme residues Ser 53, Gly 55, and Lys 72 involved in phosphate anchoring (figure generated using PDB1ATP).

The crystal contacts are in broad agreement with the observations made in the other orthorhombic mouse rC complexes (Karlsson et al., 1994). The overall structure of this polyhistidine-tagged rC is very similar to other rC structures, indicating that the 20-residue N-terminal extension does not significantly affect the protein fold. Also from the crystal packing, where the lattice contacts are strongly mediated by the peptide inhibitor, we infer that the crystals grown without the peptide inhibitor would very likely belong to a different lattice, while still maintaining the observed key intermolecular hydrophobic interactions between the enzyme residues only. This is, in fact, corroborated by the recently solved crystal structure of the binary rC:adenosine complex, where there is no peptide inhibitor. Although this complex crystallizes in a new crystal form, the indole ring of Trp 196 still stacks on Arg 133, 134 of the symmetry-related molecule (Narayana et al., manuscript in preparation). Recently it was shown that Trp 196 is a major determinant for recognition of the R-subunit of cAPK (Orellana & McKnight, 1992), while Arg 133 is an important determinant for recognition of PKI(5-24) but not R-subunit (Wen & Taylor, 1994).

DISCUSSION

General Discussion of the Nucleotide Binding Site. Several conserved motifs in the small lobe contribute to the nucleotide binding site. Of key importance is a nucleotide positioning motif composed of three parts: β-strand 1 which positions the adenine ring, the glycine-rich loop that positions the phosphates of ATP (Figure 1c), and β-strand 2 which positions the ribose (Figure 5). The three elements serve as a lid that covers the entire nucleotide and helps to position the γ-phosphate for transfer. Other elements that help to position the phosphates are Lys 72 in β-strand 3 and Lys 168 in the catalytic loop as well as Mg and Asp 184. The two strands linked by the glycine-rich loop function as a lid or a cap that locks the nucleotide into place. This lid is secured further by interactions involving residues from the C-terminal tail, a region which is not conserved in most other protein kinases. The strands, in general, do not move, while the tip of the loop is highly variable, depending on what occupies the active site cleft. This nucleotide positioning motif is conserved throughout the entire protein kinase family (Hanks & Hunter, 1995).

Loops at the Active Site Cleft. Many of the conserved residues that cluster around the active site are contained in three loops. The glycine-rich loop described above links β-strands 1 and 2 in the small lobe and helps to anchor the β- and γ-phosphates of ATP. The other two loops are in the large lobe. The catalytic loop (residues 166−171) links β-strands 6 and 7 while the Mg^{2+} positioning (DFG) loop (residues 184−186) links β-strands 8 and 9. The single-letter representation for amino acid residues 184−186 denotes DFG loop. Figure 6 shows the temperature factors for residues in the glycine-rich, catalytic, and DFG loops averaged over the backbone atoms in each case. Five structures of rC complexes are compared—the high-resolution binary complex with PKI(5−24) (Knighton et al., 1993), the PKI(5−24) and Mn_2·ATP ternary complex, the binary complex with the phosphorylated substrate peptide [{PKI-(5−24)N20A,A21SP}, where SP denotes the phosphorylated Ser residue], the ternary complex with ADP and unphosphorylated substrate peptide, and the PKI(5−24) and adenosine ternary complex described here. It can be seen that the glycine-rich loop is less ordered or more labile than the catalytic and DFG loops, in all the structures (Figure 6). This figure shows a similar trend with respect to the relative thermal factors among these loops within each structure. In the adenosine structure there are no phosphates, but the contact between the Ser 53 hydroxyl and the peptide inhibitor is maintained in a manner similar to that seen in the ternary complexes (rC:PKI(5−24):Mn_2·ATP and mC:PKI(5−24):Mn_2·AMP-PNP). The distance of 2.9 Å indicates a strong hydrogen bond. Thus occupying the adenine pocket can confer stability on the glycine-rich loop; however, it is the presence of the γ-phosphate and the Mg^{2+} ion which pulls the glycine-rich loop into its most stable conformation. The placement of this phosphate and the filling of the adenosine pocket are both critical. As mentioned above, the strong hydrogen bonds between Ser 53 and i:Ala 21, together with the movement of the glycine-rich loop, resulting in a complete and tight embedding of adenosine/ATP, support the property of synergism observed with respect to the simultaneous binding of the peptide inhibitor PKI(5−24) and ATP (Whitehouse & Walsh, 1983; Lew et al., 1997).

The thermal stability of the C-subunit, its catalytic activity, and the stability of the holoenzyme complex of the C-subunit with the RI subunit are all influenced by the occupation of the ATP binding pocket by nucleotide and metal ions (Herberg & Taylor, manuscript in preparation). There are two metal binding sites associated with the phosphates of the ATP. Catalysis is most efficient when only one metal is present; however, the thermal stability is maximized when both metals are present. Adenosine alone can confer almost

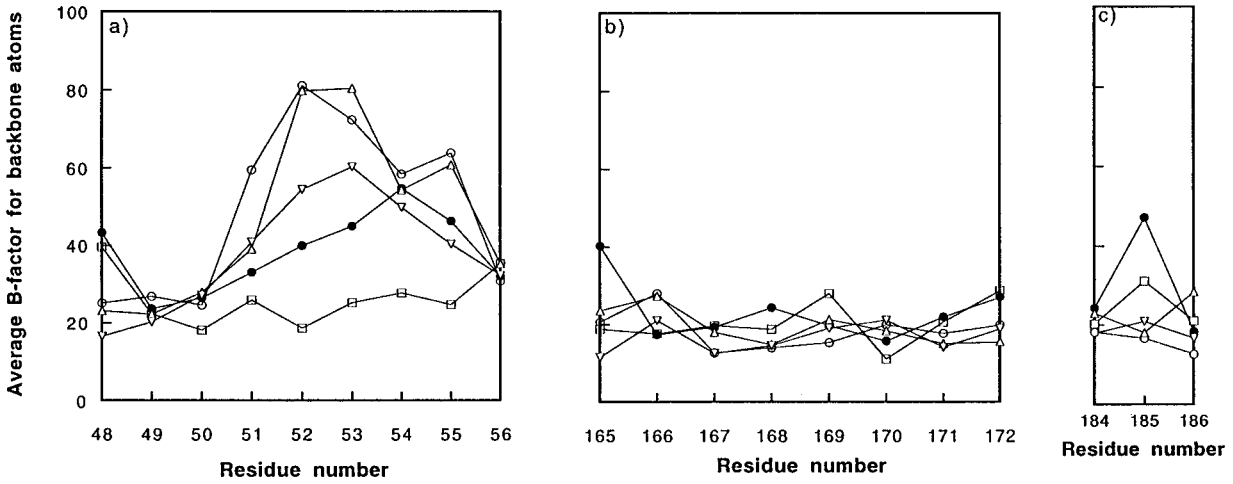

FIGURE 6: Plot of average *B*-factors for the main-chain atoms: (a) glycine-rich loop, (b) catalytic loop, and (c) DFG loop. Symbols: (●) rC:PKI(5−24): adenosine, (□) rC:PKI(5−24):Mn_2·ATP, (▽) rC:[PKI(5−24)N20A,A21S]:ADP, (○) rC:PKI(5−24), and (△) rC:[PKI(5−24)N20A,A21SP]. As seen from the graph, the trend in each of the structures is that the *B*'s in the catalytic and DFG loops are low and stable in contrast to the glycine-rich loop.

the same degree of thermal stability as Mg_2·ATP and more than either Mg·ATP or ATP. That is, occupation of the adenosine pocket is sufficient to obtain a stabilized C-subunit. In the crystal structure described here, the region which shows the most significant difference in degree of order is the glycine-rich loop; this is more ordered than in any of the other closed conformations except the Mn_2·ATP structure, suggesting that the thermal stabilization is at least in part provided by stabilization of the glycine-rich loop.

Solvent Structure in the Active Site Cleft. In addition to the adenosine, 10 water molecules are observed in the active site cleft. The average *B*-factor for these waters is 45.9 Å^2. Several of these have been observed in other crystallographic structures of the rC complexes. One of the water molecules, Wtr 415, occupies the position of the γ-phosphate of ATP in the rC:PKI(5−24):Mn_2·ATP complex (Figure 7). This water molecule bridges the side chains of Asp 166 and Lys 168, two invariant residues in the catalytic loop. The γ-phosphate that fills this site in the rC:PKI(5−24):ATP structure also hydrogen bonds to the backbone amide of Ser 53 as well as Lys 168, and this links the small and large lobes. This link is thought to be important for catalysis (Bossemeyer, 1994). In contrast to the phosphates, Wtr 415 links two of the conserved residues in the catalytic loop, Lys 168 and Asp 166, which is positioned to serve as a catalytic base leaving Ser 53. In addition, Wtr 415 interacts with the water molecule, Wtr 438, which bridges to the 5′-OH of the adenosine. The γ-phosphate of ATP makes contacts with several residues, and these interactions are thought to be critical for stabilizing the transition state. These are N of Lys 168 and the backbone amide of Ser 53 in the catalytic loop. Asp 166 in the PKS(5−24) complex hydrogen bonds with the OH of the P-site Ser in the peptide. The water molecule Wtr 415 stabilizes these two residues in the large lobe but does not H-bond to Ser 53 in the small lobe.

Wtr 375 is of particular interest. It was recently shown to be conserved in other rC structures (Shaltiel et al., manuscript in preparation). Wtr 375 was the strongest sharp peak (>5 σ) in a $F_o - F_c$ map calculated in the first round of the solvent inclusion process. This water molecule is pentacoordinated with the exocyclic O2′ of adenosine, the carbonyl oxygen of Leu 49, the carboxylate oxygen OE2 of Glu 127, the hydroxyl of Tyr 330 in the enzyme, and another water molecule, Wtr 359. Wtr 375 accepts two hydrogen bonds, one from Wtr 359 and the other from Tyr 330, and donates three hydrogen bonds (to Leu 49, Glu 127, and O2′ of adenosine), of which one is a linear hydrogen bond (to Leu 49). The other two are probably involved in the formation of three-center hydrogen bonds (Taylor et al., 1984; Fritsch & Westhof, 1991; Jeffrey & Saenger, 1994). In the rC:PKI(5−24):Mn_2·ATP and mC:PKI(5−24):Mn_2·AMP-PNP structures, the equivalent of Wtr 375 was also pentacoordinated with the O2′ of adenosine, Leu 49, Glu 127, and Tyr 330 of the enzyme, and another water molecule similar to that seen in the present structure. The importance of O2′ in nucleotide binding was observed when the ATP binding site of this kinase was mapped with 24 ATP analogues (Hoppe et al., 1978). The equivalent of Wtr 375 was still present in the binary complex rC:PKI(5−24) where there was no ATP. This conserved water molecule (Shaltiel et al., manuscript in preparation) is involved in an approximate tetrahedral arrangement with Leu 49, Glu 127, Tyr 330, and another water molecule. Because similar hydration sites are occupied in different complexes and crystallization conditions, it seems likely that binding of solvent at such sites will be maintained in solution under physiological conditions. Thus in a closed conformation with bound adenosine, ATP, AMP-PNP, or ADP, the hydroxyl of Tyr 330 is involved with a bound water-mediated interaction with the nucleoside/nucleotide. The Tyr 330 hydroxyl also makes a hydrogen bond with the P-3 Arg of the peptide inhibitor (Chestukhin et al., 1996).

Tyr 330 in the C-terminal tail and flanked by carboxylates contributes to the significant negative electrostatic character of this surface and lies outside the conserved core. In a recent study Tyr 330 was mutated to Ala, Ser, and Phe (Chestukhin et al., 1996). The mutant where Tyr was replaced with Ala had a significantly elevated K_m for ATP (from 40 to 230 μM) as well as for peptide substrate. Tyr 330 lies in a segment of the C-terminal tail that is associated with the N-terminal lobe. In the crystal structure of the "open" conformation of the mC (Zheng et al., 1993c), this section of chain was rotated away from the large lobe and remained associated with the smaller N-terminal lobe. The

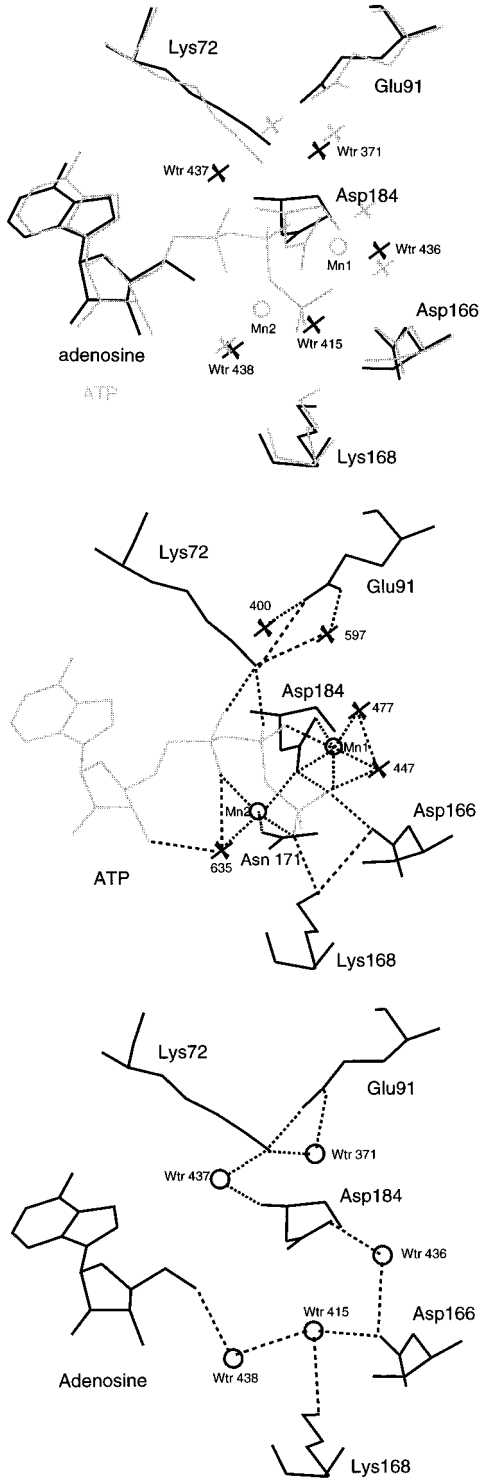

FIGURE 7: Solvent structure in the active site cleft. (a, top) rC complex with PKI(5−24) and Mn_2·ATP. The dotted lines represent interactions less than 3.5 Å. ATP is in gray; circles and asterisks represent Mn ions and water oxygens, respectively. (b, middle) The two structures rCIA (black) and rCI·ATP (gray) are superimposed using C^{α} atoms of residues 128−300. The water molecules in rCIA are labeled, and Mn ions in rCI·ATP are denoted by circles. (c, bottom) rC ternary complex with PKI(5−24) and adenosine. Wtr 415 occupies the position of the γ-phosphate in rCI·ATP.

Tyr 330 hydroxyl in that structure was 7 Å away from either the adenosine binding pocket or the peptide inhibitor. It is possible that the interactions of this Tyr via water with the ribose of the nucleotide and with the peptide contribute to the promotion of the active, "closed" conformation of the enzyme (Shaltiel et al., manuscript in preparation). Structural changes in this C-terminal region accompanying the substrate binding were proposed from CD experiments (Reed & Kinzel, 1984). In addition, chemical modifications of the sulfhydryl groups in the C-subunit, Cys 199 and Cys 343, demonstrated the malleability of this C-terminal tail (Jimenez et al., 1982).

To obtain a catalytically active C-subunit, it is necessary that the enzyme assumes a fully closed conformation in which the two lobes are brought together and the glycine-rich loop is positioned correctly. In this crystal structure which assumes a closed conformation, adenosine occupies the nucleotide binding pocket and a water molecule (Wtr 415) replaces the γ-phosphate of the ATP. The glycine-rich loop is stabilized in this structure, but the conformation and degree of order in the glycine-rich loop observed in the rCI·ATP structure is not achieved. It is this latter conformation which is the most stable conformation observed so far. Full activity of the C-subunit is obtained when only one metal site is occupied. The occupation of the second site causes a decrease in K_m for ATP but also leads to a decrease in V_{max}. The decrease in V_{max} is probably due to increased affinity for Mg·ADP, the release of which is the rate-limiting step in the chemical reaction (Adams & Taylor, 1992). Finally, it is possible that positioning of the C-terminal tail, and in particular Tyr 330, also contributes to obtaining both the stable and active conformations via its interactions with the peptide inhibitor, water, and the ribose. The C-terminal tail embedding residues 323−333 appears to play an important role in peptide recognition, nucleoside binding, and domain closure.

ACKNOWLEDGMENT

We thank Dr. Victor Ashford, Chris Nielsen, Don Sullivan, and Nick Nguyen for support at the NIH National Research Resource at UCSD multiwire-area-detector facility. We acknowledge the computing time from the San Diego Super Computer Center for X-PLOR refinements. We thank Dr. Lynn Ten Eyck for reviewing the manuscript. Sean Bell and Siv Garrod are thanked for providing high-quality purified H_6-rC and PKI(5−24), respectively.

REFERENCES

Adams, J. A., & Taylor, S. S. (1992) *Biochemistry 31*, 8516−8522.
Bhatnagar, D., Roskoski, R. J., Rosendahl, M. S., & Leonard, N. J. (1983) *Biochemistry 22*, 6310−6317.
Bossemeyer, D. (1994) *Trends Biochem. Sci. 19*, 201−205.
Bossemeyer, D., Engh, R. A., Kinzel, V., Ponstingl, H., & Huber, R. (1993) *EMBO J. 12*, 849−859.
Brunger, A. T. (1992) *X-PLOR Version 3.1 Manual: A System for X-ray Crystallography & NMR*, Yale University Press, New Haven, CT.
Cambillau, C., & Horjales, E. (1987) *J. Mol. Graphics 5*, 174−177.
Cheng, H. C., van Patten, S. M., Smith, A. J., & Walsh, D. A. (1986) *Biochem J. 231*, 655−661.
Chestukhin, A., Litovchick, L., Schourov, D., Cox, S., Taylor, S. S., & Shaltiel, S. (1996) *J. Biol. Chem. 271*, 10175−10182.
Fritsch, V., & Westhof, E. (1991) *J. Am. Chem. Soc. 113*, 8271−8277.
Grant, B. D., & Adams, J. A. (1996) *Biochemistry 35*, 2022−2029.
Hamlin, R. (1985) *Methods Enzymol. 114*, 416−452.
Hanks, S. K., & Hunter, T. (1995) *FASEB J. 9*, 576−596.
Herberg, F. W., Bell, S. M., & Taylor, S. S. (1993) *Protein Eng. 6*, 771−777.
Hoppe, J., Freist, W., Marutzky, R., & Shaltiel, S. (1978) *Eur. J. Biochem. 90*, 427−432.

Howard, A. J., Nielsen, C., & Xuong, N.-h. (1985) *Methods Enzymol. 114A*, 452−472.
Insight II User Guide, Version 2.3.9 (1994) Biosym Technologies, Inc., San Diego, CA.
Jeffrey, G. A., & Saenger, W. (1994) *Hydrogen bonding in biological structures*, Springer-Verlag, New York.
Jimenez, J. S., Kupfer, A., Gani, V., & Shaltiel, S. (1982) *Biochemistry 21*, 1623−1630.
Karlsson, R., Madhusudan, Taylor, S. S., & Sowadski, J. M. (1994) *Acta Crystallogr. D50*, 657−662.
Knighton, D. R., Zheng, J., Ten Eyck, L. F., Ashford, V. A., Xuong, N.-h., Taylor, S. S., & Sowadski, J. M. (1991a) *Science 253*, 407−414.
Knighton, D. R., Zheng, J., Ten Eyck, L. F., Xuong, N.-h., Taylor, S. S., & Sowadski, J. M. (1991b) *Science 253*, 414−420.
Knighton, D. R., Bell, S. M., Zheng, J., Ten Eyck, L. F., Xuong, N.-h., Taylor, S. S., & Sowadski, J. M. (1993) *Acta Crystallogr. D49*, 357−361.
Kraulis, P. J. (1991) *J. Appl. Crystallogr. 24*, 946−950.
Laskowski, R. A., MacArthur, M. W., Moss, D. S., & Thornton, J. M. (1993) *J. Appl. Crystallogr. 26*, 283−291.
Lew, J., Coruh, N., Tsigelny, I., Garrod, S., & Taylor, S. S. (1997) *J. Biol. Chem. 272*, 1507−1513.
Luzzati, P. V. (1952) *Acta Crystallogr. 5*, 802−810.
Madhusudan, Trafny, E. A., Xuong, N.-h., Adams, J. A., Ten Eyck, L. F., Taylor, S. S., & Sowadski, J. M. (1994) *Protein Sci. 3*, 176−187.
Orellana, S. A., & McKnight, G. S. (1992) *Proc. Natl. Acad. Sci. U.S.A. 89*, 4726−4730.
Ramachandran, G. N., & Sasisekharan, V. (1968) *Adv. Protein Chem. 23*, 283−438.
Reed, J., & Kinzel, V. (1984) *Biochemistry 23*, 968−973.
Saenger, W. (1984) *Principles of Nucleic Acid Structure*, Springer-Verlag, New York.
Slice, L. W., & Taylor, S. S. (1989) *J. Biol. Chem. 264*, 20940−20946.
Taylor, R., Kennard, O., & Versichel, W. (1984) *J. Am. Chem. Soc. 106*, 244−248.
Taylor, S. S., Buechler, J. A., & Knighton, D. R. (1990) in *Peptides and Protein Phosphorylation* (Kemp, B. E., Ed.) pp 1−42, CRC Press, Inc., Boca Raton, FL.
Taylor, S. S., Knighton, D. R., Zheng, J., Ten Eyck, L. F., & Sowadski, J. M. (1992) *Annu. Rev. Cell Biol. 8*, 429−462.
Taylor, S. S., Knighton, D. R., Zheng, J., Sowadski, J. M., Gibbs, C. S., & Zoller, M. J. (1993) *Trends Biochem. Sci. 18*, 84−89.
Tronrud, D. E., Ten Eyck, L. F., & Matthews, B. W. (1987) *Acta Crystallogr. A43*, 489−501.
Wen, W., & Taylor, S. S. (1994) *J. Biol. Chem. 269*, 8423−8430.
Whitehouse, S., & Walsh, D. A. (1983) *J. Biol. Chem. 258*, 3682−3692.
Zheng, J., Knighton, D. R., Xuong, N.-h., Parello, J., Taylor, S. S., & Sowadski, J. M. (1992) *Acta Crystallogr. B48*, 241−244.
Zheng, J., Knighton, D. R., Ten Eyck, L. F., Karlsson, R., Xuong, N.-h., Taylor, S. S., & Sowadski, J. M. (1993a) *Biochemistry 32*, 2154−2161.
Zheng, J., Trafny, E. A., Knighton, D. R., Xuong, N.-h., Taylor, S. S., Ten Eyck, L. F., & Sowadski, J. M. (1993b) *Acta Crystallogr. D49*, 362−365.
Zheng, J., Knighton, D. R., Xuong, N.-h., Taylor, S. S., Sowadski, J. M., & Ten Eyck, L. F. (1993c) *Protein Sci. 2*, 1559−1573.

BI961947+